AIR-SEA FLUXES FROM SYNTHETIC APERTURE RADAR: AN UPDATE

Todd D. Sikora
United States Naval Academy, Annapolis, MD 21402

And

Donald R. Thompson
The Johns Hopkins University Applied Physics Laboratory, Laurel, MD 20723

1. INTRODUCTION

Young et al. (2000) proposed and demonstrated a method to calculate diabatic wind speed and turbulence statistics from neutral wind speed imagery (Thompson and Beal, 2000) generated from synthetic aperture radar (SAR) data. Their method, referred to herein as the SAR method, is based on Monin-Obukhov and mixed layer similarity theory (Panofsky and Dutton, 1984; Stull, 1988). It relates the ratio of the mean to standard deviation wind speed, from the SAR-derived neutral wind speed imagery, to the static stability of the atmospheric surface layer. The scaling parameters arising from this relationship provide a stability correction to the neutral wind speed imagery in an iterative fashion. See Young et al. (2000) for an in-depth review of their method.

Upon completion of the stability correction, several of the resulting statistics (the Obukhov length ($\overline{L}$) and friction velocity ($\overline{u_*}$)) can be combined with an independent measure of the sea-surface virtual temperature ($\overline{T_v}$) to provide an estimate of the kinematic buoyancy flux ($\overline{B}$):

1) $\quad \overline{B} = -\dfrac{\overline{u_*^3 T_v}}{\overline{L}kg}$,

where k is von Kármán's constant and g is the acceleration of gravity (overbars denote values averaged over a wind speed image sub-scene).

The demonstration of the SAR method by Young et al. (2000) was accomplished using *in situ* turbulence data gathered during the second High Resolution Remote Sensing (HI-RES 2) project as ground truth. The comparisons presented in Young et al. (2000) were for data collected during rather quiescent synoptic scale and statically unstable microscale atmospheric conditions (i.e., light winds and negative air-sea temperature differences).

Sikora et al. (2000) furthered the demonstration / testing of the SAR method by expanding the environmental conditions for such to more baroclinic regimes. Sikora et al. (2000) relied on National Ocean and Atmospheric Administration (NOAA) buoys to provide a means of ground truth and only investigated the performance of the SAR method in the calculation of $\overline{L}$ and the drag coefficient ($\overline{C_d}$). Although NOAA buoys do not provide such turbulence statistics, they do provide enough *in situ* data for input into the bulk flux algorithm arising from Tropical Ocean Global Atmosphere- Coupled Ocean Atmosphere Response Experiment (TOGA-COARE) (Fairall et al. 1996). The TOGA-COARE bulk flux algorithm, therefore, provided the "ground truth" for comparisons presented in Sikora et al. (2000).

Unlike the Young et al. (2000) study, the work reported in Sikora et al. (2000) did not include spectral filtering of the neutral wind speed imagery prior to the generation of their turbulence statistics. However, Sikora et al. (2000) smoothed the pixel size of the SAR imagery to 300 m. This choice of pixel size and smoothing arose from the study of Mourad et al. (2000), who found that doing so resulted in a close fit between the wind spectrum resulting from a SAR image and that developed using low-level turbulence measurements gathered from an aircraft flying over the imaged area.

The purpose of this paper is to report the results of the testing of the SAR method that has been accomplished since the publication of Sikora et al. (2000). The present research continues the work of Sikora et al. (2000), conducted using Radarsat-1 overpasses off the east coast of the United States between October 1996 and March 1997. While several of the case studies that we present below overlap with those presented in Sikora et al. (2000), we deviate from their work in that the results for the ratio of reference height (z) to $\overline{L}$ as well as for $\overline{B}$ are presented in place of $\overline{L}$ and $\overline{C_d}$.

2. DATA

The SAR data set employed in the present research comes from a 12-overpass Radarsat-1 narrow ScanSAR collection initiative by the Ocean Remote Sensing Group at the Johns Hopkins University Applied Physics Laboratory. All 12 overpasses can be seen at (http://fermi.jhuapl.edu/en_sar.html). For each overpass, we inspected data from all NOAA buoys located within the imaged area, as well as data from a Woods Hole Oceanographic Institution mooring operating in support of the Coastal Mixing and Optics (CMO) experiment, in order to choose sub-scenes for case studies. Case studies were chosen if the air-sea temperature difference at a reporting station was less than $-1\ ^{\circ}$C at the time of the corresponding overpass. This criterion was chosen because the SAR method is intended for use in the presence of statically unstable environments. This selection process resulted in 13 cases studies from 9 overpasses.

Table 1 summarizes the air-sea temperature

Table 1. Summary of air-sea temperature difference and wind data gathered at the buoys for each of the 13 case studies.

Buoy	Date	Case Study	Delta T (^{o}C)	Wind Speed (ms^{-1})	Wind Direction (^{o}T)
44004	10/10/96	A	-1.4	9.0	262
41001	10/13/06	B	-4.4	3.9	016
44004	01/14/97	C	-9.4	8.7	290
44008	01/14/97	D	-4.1	8.1	285
CMO	01/14/97	E	-4.7	9.5	285
41001	01/17/97	F	-14.8	8.2	294
44025	01/17/97	G	-14.2	10.9	265
CMO	02/07/97	H	-1.9	7.0	290
41001	02/10/97	I	-3.6	11.0	123
44025	02/10/97	J	-3.4	5.7	290
44014	02/13/97	K	-2.5	8.5	084
41001	03/06/97	L	-4.4	12.1	295
44014	03/09/97	M	-2.2	5.7	086

difference and wind data gathered at the *in situ* stations for each of the 13 case studies. Because all SAR overpasses occurred around 2300 UT, the buoy data found in Table 1 is the 8-minute average reported by the National Data Buoy Center for that time for any particular case study. That for the CMO mooring is the 15-minute average reported for that time for any particular case study. A map of the buoy stations cited in Table 1 can be found at http://seaboard.ndbc.noaa.gov/. The CMO mooring was located at 40.5 N , -70.5 E.

The air-sea temperature difference ranged from –1.4 to -14.8 ^{o}C, the wind speed ranged from 3.9 to 12.1 ms^{-1}, and the wind directions covered every quadrant of the compass. Therefore, the environmental conditions for the present research were conducive for robust testing of SAR method.

Figure 1 shows imagettes of 10 m neutral wind speed from which each of the 13 sub-scenes were chosen. Each imagette is composed of 300 m pixels, has dimensions of 105 km by 105 km, and is oriented so that the top of the page is directed towards 348 ^{o}T. Notice that within many of these imagettes, the mottled SAR signature of cellular convection (Sikora et al., 1995; Zecchetto et al., 1998) is evident. These neutral wind speed imagettes were created following the procedure outlined in Thompson and Beal (2000). However, because calibration coefficients from the early Radarsat-1 imagery employed herein are in question, we first scaled the cross section from a 21 km square centered on the *in situ* station for each original SAR imagette such that resulting 10 m neutral wind speed, averaged over the 21 km square, equaled that from the corresponding *in situ* station.

The sub-scenes used for our case studies were developed from these imagettes by invoking Taylor's hypothesis using the wind speeds reported in Table 1, thus allowing the temporal data reported by the *in situ*
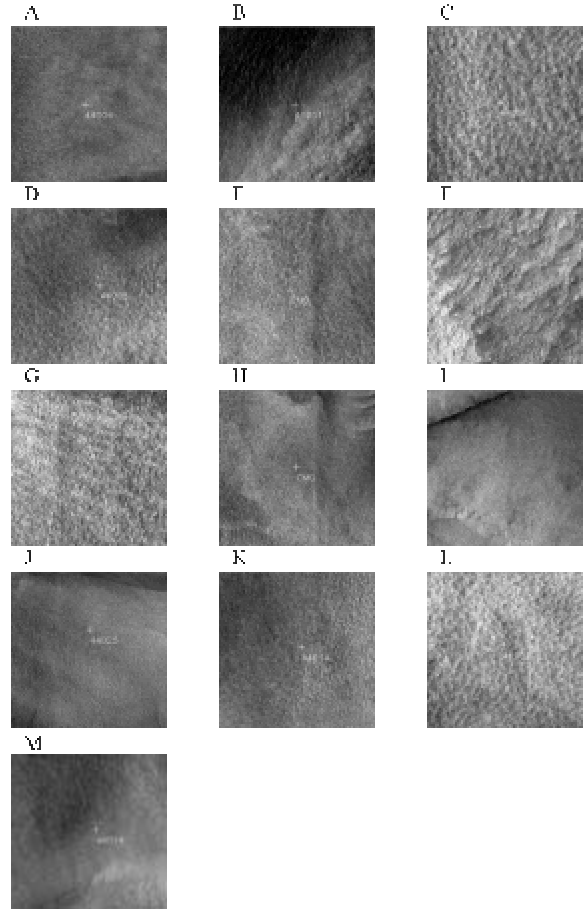

Figure 1. Imagettes of the 10 m neutral wind speed from which each of the 13 sub-scenes were chosen. Letters correspond to separate case studies found within Table 1.

stations to be compared to the spatial data found within the wind speed imagery. The average area of all 13 sub-scenes is 18 km^2. All sub-scenes were oriented such that one of their axes paralleled the average wind direction reported by the corresponding *in situ* station.

Unlike what was presented in Sikora et al. (2000), the results found below for the SAR method constitute average values of $z/\overline{L}$ and $\overline{B}$ for a 3-by-3 grid of sub-scenes centered on the *in situ* station for a particular case study. This was done in order to provide a more robust sample of both statistics while, at the same time, allowing us to assess their variability over the area of interest.

As was done by Sikora et al. (2000), ground truth turbulence data reported herein comes from the TOGA-COARE bulk flux algorithm, using the data reported by the *in situ* stations as input. Because humidity measurements were not reported by the NOAA buoys, but are required for calculation of the bulk statistics, we assumed 100% relative humidity for all of our case studies. We also used the *in situ* data and assumed

100% relative humidity when calculating $\overline{T_v}$ for input into equation 1.

3. RESULTS AND DISCUSSION

Figure 2 shows the TOGA-COARE / SAR method comparisons for $z/\overline{L}$ (a) and $\overline{B}$ (b). The slope and y intercept from simple linear regression are also shown on each plot. The overall correlation for both sets of comparisons is quite good. The correlation coefficient for $z/\overline{L}$ is 0.77 while that for $\overline{B}$ is 0.95. The mean difference and root mean square difference (COARE results – SAR results) for the $z/\overline{L}$ comparisons are –0.008 and 0.119 respectively. That for the $\overline{B}$ comparisons is 0.030 ms^{-1}K (mean difference) and 0.039 ms^{-1}K (root mean square difference).

Examining the two plots more closely and accepting the TOGA-COARE data as truth, one finds that the SAR method tends to underestimate $\left|z/\overline{L}\right|$ for weakly statically unstable environments and vice versa. Turing to the $\overline{B}$ comparisons, the SAR method tends to provide a slight underestimate for all ranges of static stability examined.

Scrutinizing the SAR method, we find that the value of $z/\overline{L}$ it produced, averaged over all 13 case studies, is –0.15. The standard deviation of $z/\overline{L}$ from the SAR method, averaged over all 13 case studies, is 0.11. The corresponding values for $\overline{B}$ are 0.046 ms^{-1}K (average) and 0.034 ms^{-1}K (standard deviation). Hence, there was quite a bit of relative variability in the output from SAR method for both statistics. This result was somewhat expected. By examining Figure 1, one can see that for several of the case studies, there was a large amount of variability in the degree of mottling seen in the neutral wind field about the buoys (e.g., large pattern changes are evident in Figure 1b). This lack of homogeneity resulted in large differences in the estimates of $z/\overline{L}$ and $\overline{B}$ from one of the 9 sub-scenes to another for the same case study. We cannot, therefore, simply attribute the large amount of variability noted in our results to some deficiency in the SAR method or our application of it. It may be that the observed variability is real.

Potential sources of error for the SAR method, beyond those discussed above, have been noted in Young et al. (2000) as well as in Sikora et al. (2000). Here, we outline the more probable candidates. For one, any extraneous variance in the wind speed imagery other than that owing to the wind (e.g., that due to oceanographic phenomena and speckle) will cause an incorrect assessment of the turbulence statistics. Implicit in the smoothing of the SAR imagery to 300 m was the attempt to diminish or remove such variance. However, degradation of the resolution of the SAR
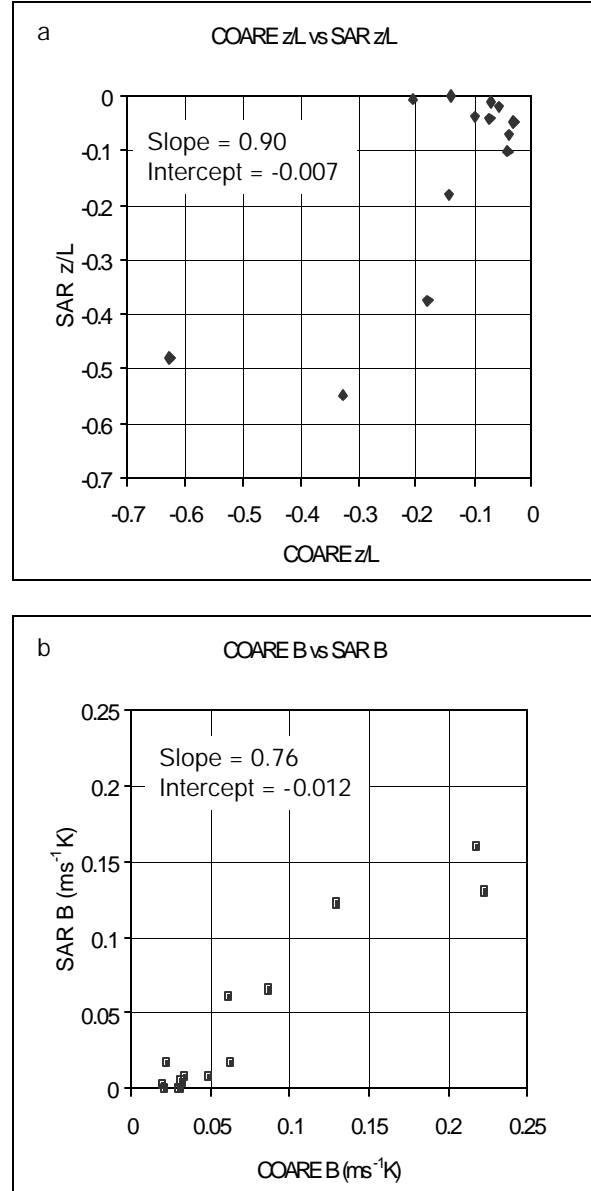

Figure 2. TOGA-COARE / Young et al. (2000) comparisons for (a) $z/\overline{L}$ and (b) $\overline{B}$.

imagery by smoothing to 300 m may inadvertently eliminate a significant amount of variance owing to the wind under certain circumstances. Only the limited Mourad et al. (2000) study justifies such an approach. Another potential source of error includes the presence certain sea states that can affect the near-surface turbulence in such a way as to cause a breakdown of Monin-Obukhov similarity theory (e.g., Drennan et al. 1999). Finally, the proper choice of $\overline{Z_i}$ is imperative for the correct assessment of $\overline{L}$, on which the SAR method hinges. To the best of our knowledge, there has been no systematic study addressing the ability of diagnosing

$\overline{Z_i}$ from SAR data beyond the study presented in Sikora et al. (1997).

4. SUMMARY

A similarity theory-based method (referred to as the SAR method) for calculating turbulence statistics from SAR-derived neutral wind speed imagery (first presented in Young et al. (2000)) was tested. We concentrated on its ability to yield proper estimates of the ratio of reference height to Obukhov length ($z/\overline{L}$) and kinematic buoyancy flux ($\overline{B}$), where the overbars denote averages over a sub-scene of the wind speed image. The TOGA-COARE bulk flux algorithm, fed with buoy and mooring data corresponding in space and time to the wind speed image sub-scenes, provided a comparison data set. The $z/\overline{L}$ and $\overline{B}$ values derived from the SAR method that are reported herein are averages from a 3-by-3 sub-scene grid centered on a particular *in situ* station. Thirteen cases studies were examined covering an air-sea temperature difference range of −1.4 to -14.8 $^{\circ}$C and a wind speed range of 3.9 to 12.1 ms^{-1} (as measured by the *in situ* stations).

The correlation coefficient for the $z/\overline{L}$ comparison is 0.77 while that for $\overline{B}$ is 0.95. The mean difference and root mean square difference (COARE results − SAR results) for the $z/\overline{L}$ comparisons are −0.008 and 0.119 respectively. That for the $\overline{B}$ comparisons is 0.030 ms^{-1}K (mean difference) and 0.039 ms^{-1}K (root mean square difference).

Accepting the TOGA-COARE data as truth, the SAR method tends to underestimate $z/\overline{L}$ for weakly statically unstable environments and vice versa. For the $\overline{B}$ comparisons, the SAR method tends to provide a slight underestimate for all ranges of static stability examined. The value of $z/\overline{L}$ produced by the SAR method, averaged over all 13 case studies, is −0.15. The standard deviation of $z/\overline{L}$ from the SAR method, averaged over all 13 case studies, is 0.11. The corresponding values for $\overline{B}$ are 0.046 ms^{-1}K (average) and 0.034 ms^{-1}K (standard deviation).

Potential sources of error for the SAR method include the neutral wind estimates derived from the SAR imagery, the sea state, and the improper diagnosis of the mixed layer depth from the neutral wind speed imagery.

5. REFERENCES

Drennan, W. M., K. K. Khama, and M. A. Donelan, 1999: On momentum flux and velocity spectra over waves, *Boundary-Layer Meteorol.*, **92**, 489-515.

Fairall, C. W., E. F. Bradley, D. P. Rogers, J. B. Edson, G. S. Young, 1996: Bulk parameterization of the air-sea fluxes for tropical ocean-global atmosphere response experiment. *J. Geophys. Res.*, **101**, 3747-3764.

Mourad, P. D., D. R. Thompson, D. C. Vandemark, 2000: Extracting fine-scale wind fields from synthetic aperture radar Images of the ocean surface, *Johns Hopkins University APL Technical Digest*, **21**, 108-115.

Panofsky, H. A., and J. A. Dutton, 1984: *Atmospheric Turbulence*. Wiley-Interscience, 397 pp.

Sikora, T. D., G. S. Young, R. C. Beal, and J. B. Edson, 1995: On the use of spaceborne synthetic aperture radar imagery of the sea surface in detecting the presence and structure of the convective marine atmospheric boundary layer. *Mon. Wea. Rev.*, **123**, 3623-3632.

Sikora, T. D., G. S. Young, H. N. Shirer, and R. D. Chapman, 1997: Estimating convective boundary layer depth from microwave radar imagery of the sea surface. *J. Appl. Meteorol.*, **36**, 833-845.

Sikora, T. D., D. R. Thompson, and J. C. Bleidorn, 2000: Testing the diagnosis of marine atmospheric boundary layer structure from synthetic aperture radar, *Johns Hopkins University APL Technical Digest*, **21**, 94-99.

Stull, R. B., 1988: *An Introduction to Boundary Layer Meteorology*. Kluwer Academic Publishers, 666 pp.

Thompson, D. R., and R. C. Beal, 2000: Mapping mesoscale and submesoscale wind fields using synthetic aperture radar, *Johns Hopkins University APL Technical Digest*, **21**, 58-67.

Young, G. S., T. D. Sikora, and N. S. Winstead, 2000: Inferring marine atmospheric boundary layer properties from spectral characteristics of satellite-borne SAR imagery, *Mon. Wea. Rev.*, **128**, 1506-1520.

Zecchetto, S., P. Trivero, B. Fiscella, and P. Pavese, 1998: Wind stress structure in the unstable marine surface layer detected by SAR, *Boundary-Layer Meteorol.*, **86**, 1-28.